Journal of Inorganic and Organometallic Polymers and Materials (2024) 34:864–873
https://doi.org/10.1007/s10904-023-02860-0

RESEARCH

Incorporating of Cobalt into UiO-67 Metal–Organic Framework for Catalysis CO_2 Transformations: An Efficient Bi-functional Approach for CO_2 Insertion and Photocatalytic Reduction

F. Al-dolaimy[2] · Mazin Hadi Kzar[3] · Shaymaa Abed Hussein[4] · Hala Bahir[5] · Abdul-hameed M. Hamoody[6] · Ashour H. Dawood[7] · Maytham T. Qasim[8] · Ashwaq Talib Kareem[9] · Ahmed Hussien Alawadi[10,11,12] · Ali Alsaalamy[1] · Russual Riyad[5]

Received: 12 August 2023 / Accepted: 5 September 2023 / Published online: 27 September 2023

Abstract

Carbon dioxide (CO_2) transformation is a cutting-edge technology to eliminate greenhouse effects and produce valuable chemicals as well as fuels. Herein, we report an elaborate engineering for improving the efficiency of Zr-based Bipy-UiO-67 metal–organic framework (ZBU) in CO_2 transformations. As demonstrated, tuning the catalytic performance by incorporating Co into ZBU (ZBU-Co) was realized as a practical strategy to affect the CO_2 insertion to epoxides in terms of conversion, green procedure, recyclability, chemical/thermal stability, time, and energy. Also, extending the diversity of the reaction to bulky epoxides showed that increasing temperature is an effective remedy for achieving complete conversion. Importantly, in comparison with the homogeneous and heterogeneous counterparts, ZBU-Co illustrated superior results. On the other hand, ZBU-Co exhibited potential application in photocatalytic reduction of CO_2, endowing bi-functional feature to the catalytic system. Accordingly, higher CO_2 adsorption capacity and CO evolution were recorded for ZBU-Co compared to the pristine ZBU. Furthermore, the ability to recover the catalyst for four cycles is a valuable characteristic from environmentally/eco-friendly aspects, which further proves the versatility of the modified MOF in the photocatalytic reaction. Overall, ZBU-Co is considered a promising candidate for CO_2 transformations due to the several advantages in CO_2 insertion and photocatalytic reduction.

✉ Ali Alsaalamy
alihashimalsalamy78@gmail.com

1 College of Technical Engineering, Imam Ja'afar Al-Sadiq University, Al-Muthanna 66002, Iraq

2 Al-Zahraa University for Women, Karbala, Iraq

3 College of Physical Education and Sport Sciences, Al-Mustaqbal University, Hillah, Babil 51001, Iraq

4 Department of Medical Engineering, Al-Manara College for Medical Sciences, Amarah, Maysan, Iraq

5 Medical Technical College, Al-Farahidi University, Baghdad, Iraq

6 Department of Medical Engineering, Al-Hadi University College, Baghdad 10011, Iraq

7 Department of Medical Engineering, Al-Esraa University College, Baghdad, Iraq

8 Department of Anesthesia, College of Health and Medical Technololgy, Al-Ayen University, Thi-Qar, Iraq

9 College of Pharmacy, National University of Science and Technology, Nasiriyah, Dhi Qar, Iraq

10 College of Technical Engineering, The Islamic University, Najaf, Iraq

11 College of Technical Engineering, The Islamic University of Al Diwaniyah, Al Diwaniyah, Iraq

12 College of Technical Engineering, The Islamic University of Babylon, Babylon, Iraq

Graphical Abstract

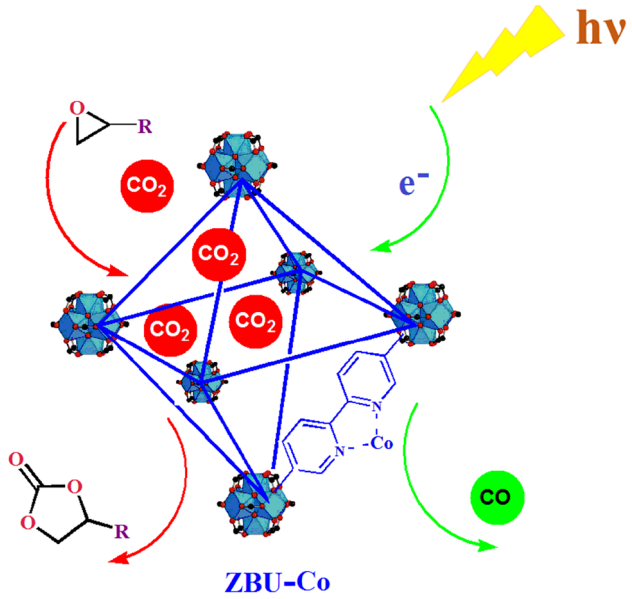

Keywords CO_2 transformation · Metal–organic frameworks · UiO-67 MOF · Photocatalytic reduction · CO_2 insertion

1 Introduction

In the twenty-first century, there is a growing concern about the excessive emission of carbon dioxide into the atmosphere [1–3]. This is related to the rapidly increasing number of inhabitants, human activities, and consumption of fossil fuels. Global warming and climate change are two serious problems that result from atmospheric CO_2 emissions [4, 5]. One of the important disadvantages of CO_2 for the global environment is the adsorption of CO_2 by oceans and seas, which causes a rise in seawater acidity [6, 7]. On the other hand, CO_2 is an essential requirement for plants that use it in photosynthesis to form organic molecules and oxygen [8, 9]. In the past years, numerous attention was drawn to the transformation of CO_2 into valuable chemical products such as carbon monoxide (CO) [10], formic acid [11, 12], methane [13, 14], methanol [15–17], and ethanol [18, 19]. In industry, CO_2 plays a vital role in producing many compounds, including drugs, fragrances, and fuels [20–24]. In particular, CO is used as fuel for heat, light, and manufacturing of organic chemicals [25, 26]. As a result, considerable efforts have been dedicated to physically absorbing CO_2 for storage and chemically converting CO_2 to other chemicals [27–29]. Among the utilized methods, photocatalytic reduction by primarily using sunlight energy and CO_2 insertion into the epoxide are ideal approaches for transforming CO_2 into fine chemicals [30–32]. One of the promising candidates for CO_2 transformation is metal–organic frameworks (MOFs) [33–35]. MOFs are a class of crystalline porous coordination polymers built-up of metal cluster nodes interconnected with multi-dentate organic linkers [36]. Benefiting from their outstanding chemical and physical properties, such as high surface area and pore volume, and tunable structure, MOFs have emerged as a mediate for various applications, including drug delivery [37], catalyst [38], sensing [39, 40], separation [41], adsorption [42], etc. Among the MOF-based porous materials, UiO-based MOFs are a class of materials with Zr cluster and phenyl-dicarboxylate ligands [43]. Zr-UiO-67-Bipydc (ZBU) can be utilized as a platform for the post-synthetic method (PSM) to incorporate secondary metals such as Co, Mn, Ru, Rh, etc. [44]. PSM of ZBU with metals provides a versatile tool for improving catalytic conversion, like CO_2 fixation [45, 46]. Also, there are a few reports on ZBU@metal (Co, Re, Ru, Rh, Ni, Mn, Pt, and Cu) with high conversion in photocatalytic CO_2 reduction. [47–55]. In this report, we synthesized a Co-modified ZBU (ZBU-Co) by PSM method under a solvothermal condition (Fig. 1). The rich nature of catalytic activation modes in the afforded MOF prompted us to employ it in CO_2 transformations. First, we envisioned that multiple Lewis acid/Lewis base sites in the as-synthesized ZBU-Co can conduct CO_2 insertion into the epoxides. Fortunately, ZBU-Co showed promising results in the production of cyclic carbonate adducts. Next, we hypothesized that Co moiety in ZBU-Co can also play the role of charge transfer medium in photocatalytic reaction. To our delight, further investigation revealed

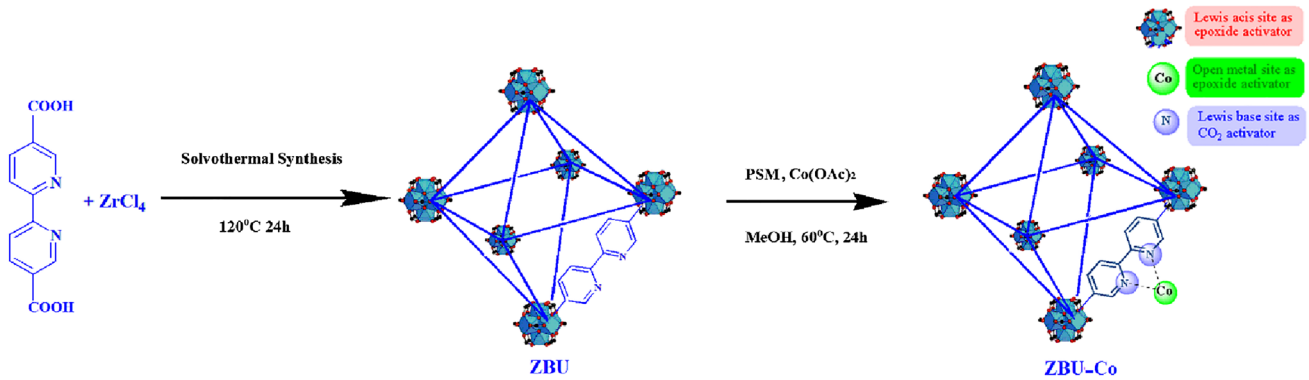

Fig. 1 Synthetic procedure of ZBU-Co via PSM and schematic illustration of ZBU-Co catalytic functions

that ZBU-Co offers a practical photocatalytic approach for the reduction of CO_2 to CO. Therefore, ZBU-Co represents a potential candidate for CO_2 transformations featuring bi-functional catalytic manner, which is unprecedented in MOFs catalysis CO_2 transformations [44]. According to our results, in both of the CO_2 transformations, ZBU-Co exhibited superior catalytic performance compared to the pristine ZBU and homogeneous analogs. Spectral and instrumental analysis including XRD, TGA, SEM, BET, ICP, XPS, fluorescence, and ^{1}H NMR were employed to get insight into the catalytic activity of the MOF.

2 Results and Discussion

2.1 Characterization of ZBU-Co

First, powder X-ray diffraction (PXRD) pattern of ZBU and ZBU-Co demonstrated the isoreticular and crystalline nature of the MOFs (Fig. 2a). Additionally, the crystallinity was well retained after post-metallation. To the finding the permanent porosity and calculate the surface area of the MOFs, N_2 adsorption–desorption isotherms at 77 K were performed. As shown in Fig. 2b, the isotherms of both MOFs exhibited type I, which were identified as microporous materials. At relative low pressures ($P/P_0 < 0.1$) and high relative pressure ($P/P_0 > 0.99$), the N_2 adsorption amount of ZBU was 455 and 800, respectively. Also, 234 and 390 $cm^3\ g^{-1}$ were obtained for N_2 adsorption of ZBU-Co (($P/P_0 < 0.1$) and ($P/P_0 > 0.99$), respectively). Moreover, the Brunauer−Emmett−Teller (BET) and Langmuir surface areas were calculated 1098 and 1800 $cm^3\ g^{-1}$ for ZBU and 603, 972 $cm^3\ g^{-1}$ for ZBU-Co, respectively. Thermal stability evaluation of MOFs was investigated by thermal gravimetric analysis (TGA) in air atmosphere at the range of 30–800 °C (Fig. 2c). TGA curves of ZBU and ZBU-Co exhibited 20% decomposition in the range of 30–500 °C for ZBU and 30–400 °C for ZBU-Co, which can be assigned to the solvent and residual molecules. The second weight loss occurred in the range of 500–600 °C for ZBU and 400–500 °C for ZBU-Co, which can be attributed to the complete decomposition of the frameworks. These data illustrate the remarkable thermal stability of the MOFs. SEM images of the MOFs exhibited cubic nanoparticles before and after metalation (Fig. 2d). The elemental analysis of ICP-OES (inductively coupled plasma optical emission spectroscopy) and XPS (X-ray photoelectron spectroscopy) has proven the successful loading of Co into the ZBU. The atomic ratio of cobalt in ZBU-Co exhibited that for each Zr atom in the cluster, there is one Co atom, so the atomic ratio of Zr/Co was obtained 1:0.3 wt%. Furthermore, XPS analysis demonstrated the presence of elements in the composite. As illustrated in Fig. 3, the XPS spectrum of the ZBU-Co exhibited the presence of Co, Zr, C, Cl, O, and N. The main peaks at 795 eV and 780 eV are shown attributed to Co^{2p}, corresponding to $^2P_{1/2}$, and $^2P_{3/2}$ of Co^{2+}, respectively. [56, 57] The production rate of CO was detected using a gas chromatograph (GC) by injection of 5 mL gas into the reactor at 1 h interval.

2.2 Catalytic Studies

2.2.1 CO_2 Insertion Into Epoxides

As depicted in Fig. 1, ZBU-Co takes advantage of various activation modes to improve CO_2 capture and fixation.

Zr-clusters and incorporated Co open-metal sites are Lewis acid centers capable of activation of epoxides. Moreover, N-donors sites in bi-pyridine linkers are considered as Lewis base sites for CO_2 activation [58]. To evaluate the dual activation mode of ZBU-Co (Zr and Co centers) in the conversion of CO_2 to cyclic carbonates, epichlorohydrin (ECH) was selected as a model substrate. The conversion efficiency of the catalysts was analyzed by ^{1}H NMR (See Supporting Information File) First, the effect of the molar ratio of ZBU-Co and TBAB (co-catalyst) on the conversion of ECH to the desired adduct 1,3-dioxolane-2-one was

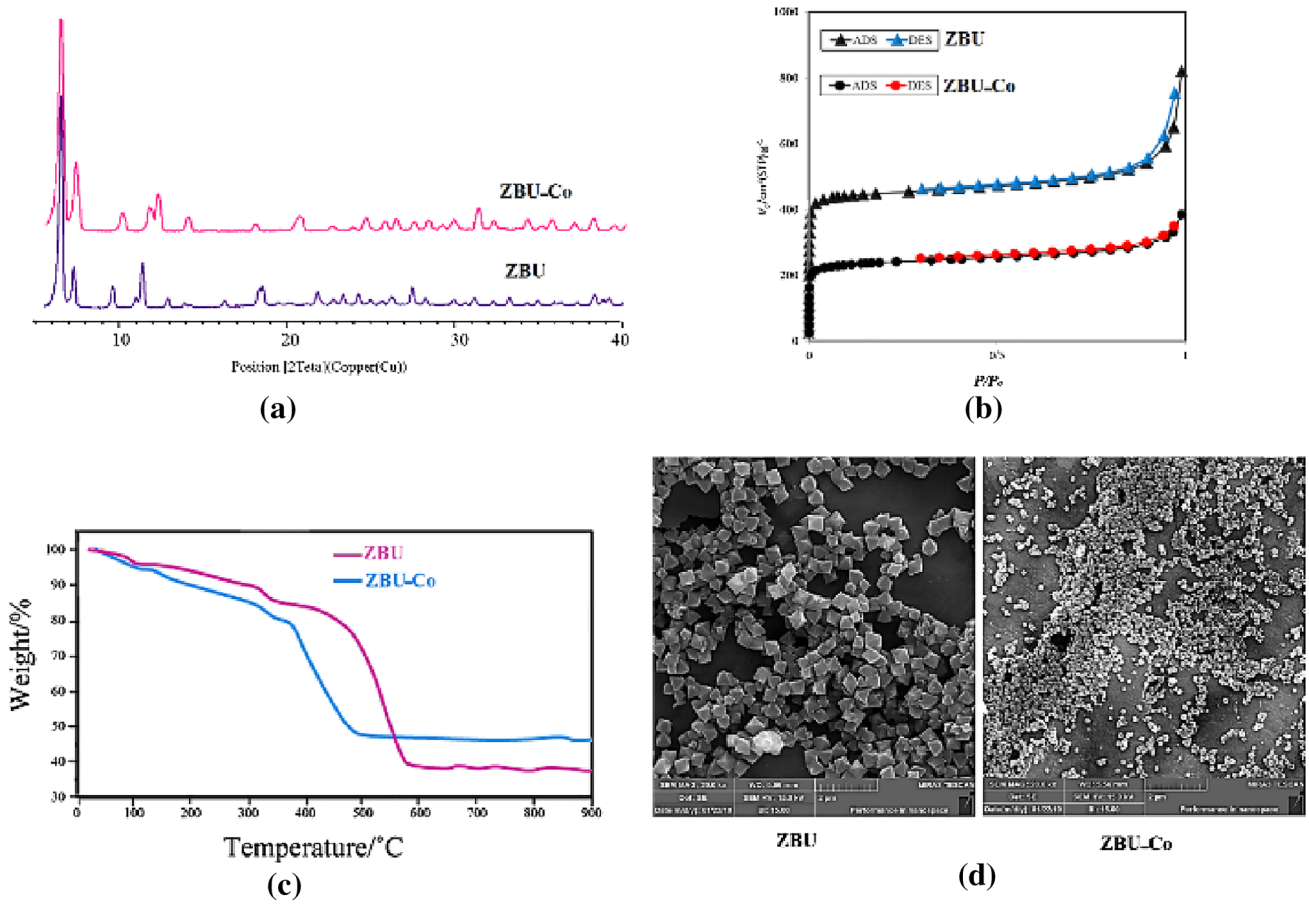

Fig. 2 **a** PXRD pattern, **b** adsorption and desorption isotherms of N_2 at 77 K, **c** TGA profiles at air condition, and **d** SEM images of ZBU and ZBU-Co

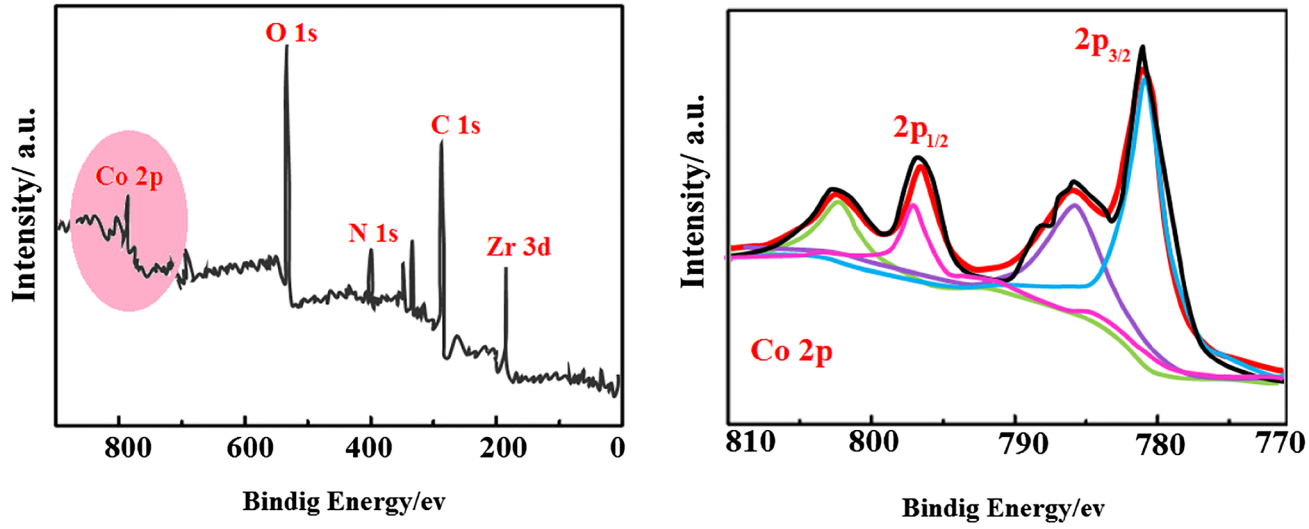

Fig. 3 High-resolution XPS spectrum of ZBU-Co

investigated (Table 1). Accordingly, as the molar ratio of TBAB increases from 1 to 3 mol%, the catalytic conversion increases significantly from 10 to 99% (Table 1, entries 1–3). Then, by lowering the amount of catalyst from 0.5 to 0.1 mol%, the catalytic conversion decreased from 99 to 43% (Table 1, entries 3–5). No catalytic conversion was observed upon removal of the co-catalyst from the reaction mixture (Table 1, entry 6). Also, removal of ZBU-Co from the reaction drastically reduced the conversion from 99 to 38% (Table 1, entry 7). Finally, trying the reaction with less than 2 mmol ECH showed a decrease in efficiency (Table 1, entry 8). Consequently, performing the reaction under CO_2 (1 bar), tetrabutylammonium bromide (TBAB) (3 mol%), ECH (2 mmol), and 0.5 mol% ZBU-Co at room temperature for 6 h was established as an optimized condition.

With optimal conditions in hand, we compared the catalytic performance of ZBU-Co with different homogeneous and heterogeneous catalysts under the considered condition. Based on our experiments, a dramatic decrease in conversion was observed as a result of conducting the reaction by various homogeneous catalysts, including $ZrCl_4$ and $Co(OAc)_2$ as Lewis acid, and 2,2′-Bipy-5,5′-dicarboxylic acid as Lewis base (Table 2, entries 3–5). Additionally, the pristine ZBU exhibited a catalytic conversion of 74%, while ZBU-Co showed superior activity toward CO_2 insertion with complete conversion (Table 2, entries 1–2).

Next, to investigate the efficiency of the catalytic system in diversity-oriented epoxides, a range of epoxides were tested in the CO_2 insertion reaction under the optimized conditions (Table 3). As demonstrated, bulkier epoxides exhibited lower efficiency compared to ECH (Table 3, Figure S20-S25). This can be attributed to the steric constraints that affect the diffusion rate of the substrates in the MOF pores [59]. Therefore, it can be concluded that the catalytic reaction occurs mostly in the MOF pores. To enhance the catalytic efficiency of the bulky epoxides, the temperature was increased from 25

Table 1 Investigation the optimal conditions for the catalytic synthesis of 1,3-dioxolane-2-one

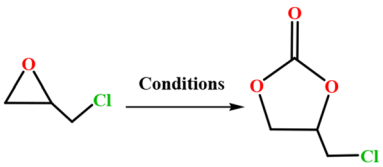

Entry	Catalyst (% mol)	TBAB (% mol)	Conversion (%)[a]
1	0.5	1	10 ± 3
2	0.5	2	43 ± 2
3	0.5	3	> 99 ± 1
4	0.2	3	53 ± 3
5	0.1	3	43 ± 1
6	0.5	0	No conv
7	0	3	38 ± 1
8[b]	0.5	3	64 ± 2

[a]Reaction condition: ECH (2 mmol), 1 bar CO_2, Room temperature, 6 h

[b]The reaction was conducted with 1.5 mmol ECH

Table 2 Evaluation of homogeneous and heterogeneous catalysts in cycloaddition of CO_2 with ECH

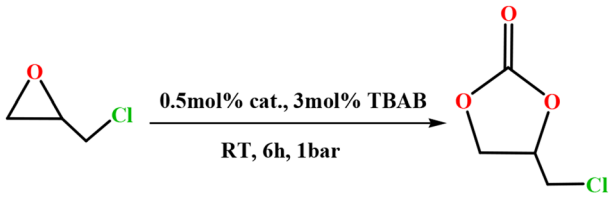

Entry	Catalysts	Conversion (%)[a]	TON	TOF (h^{-1})
1	ZBU	74 ± 1	74	6.45
2	ZBU-Co	**> 99 ± 1**	99	8.22
3	2,2′-Bipy-5,5′-dicarboxilic acid	39 ± 3	39	3.16
4	$ZrCl_4$	49 ± 2	49	4.15
5	$Co(OAc)_2$	38 ± 2	38	3.19

Reaction conditions: ECH (2 mmol), catalysts (0.5 mol% based on open metal sites), n-Bu_4NBr (3 mol%), 1 bar CO_2, Room temperature (ca. 29 °C), 6 h

Bold indicates the highest conversion distincts from other data

[a]Determined by liquid NMR in $CDCl_3$

Table 3 Cycloaddition reaction of CO_2 with various epoxides

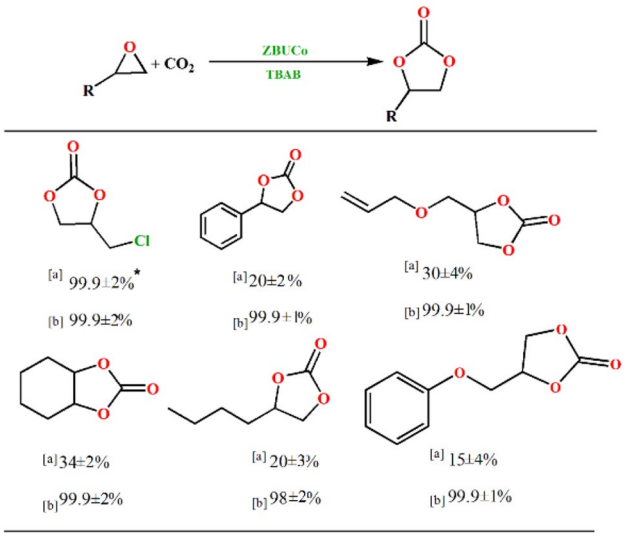

*Determined by NMR in $CDCl_3$

[a]Epoxide (2 mmol), 1 bar CO_2, Room temperature, 4 h,

[b]Epoxide (2 mmol), 1 bar CO_2, Room temperature, 4 h, 40 °C

to 40 °C. Successfully, all of the epoxides exhibited complete conversion (Table 3).

The versatility of ZBU-Co in this reaction was further proved by leaching test. Accordingly, no catalytic activity was observed by removing the catalyst after 2 h. Thus, it can be rationalized that no leaching occurred at the active catalyst sites (Fig. 4a). In addition, to investigate the chemical stability of ZBU-Co, a recyclability test was performed (Fig. 4b). As seen in Fig. 4c, the remaining PXRD patterns of the recovered catalyst showed remarkable stability after five catalytic cycles (Figure S26-30).

2.2.2 Photocatalytic Conversion of CO_2 to CO

To evaluate the efficiency of photocatalytic CO_2 reduction in the MOFs, CO_2 adsorption experiments were performed on ZBU and ZBU-Co at 298 K. During the CO_2 reduction process, CO_2 molecules were absorbed by the catalytic centers (Co). The CO_2 reduction efficiency can be attributed to the amount of CO_2 adsorbed. Therefore, MOFs with higher CO_2 capacity would exhibit higher catalytic conversion. As shown in Fig. 5, ZBU-Co had a CO_2 adsorption capacity of 36.7 $cm^3\ g^{-1}$, which was higher than the CO_2 adsorption capacity of ZBU (22.2 $cm^3\ g^{-1}$) (Fig. 5).

Next, the ability of light absorption was evaluated using UV–Vis diffuse reflectance spectroscopy (DRS). As shown in Fig. 6, both complexes showed photo-absorption from UV

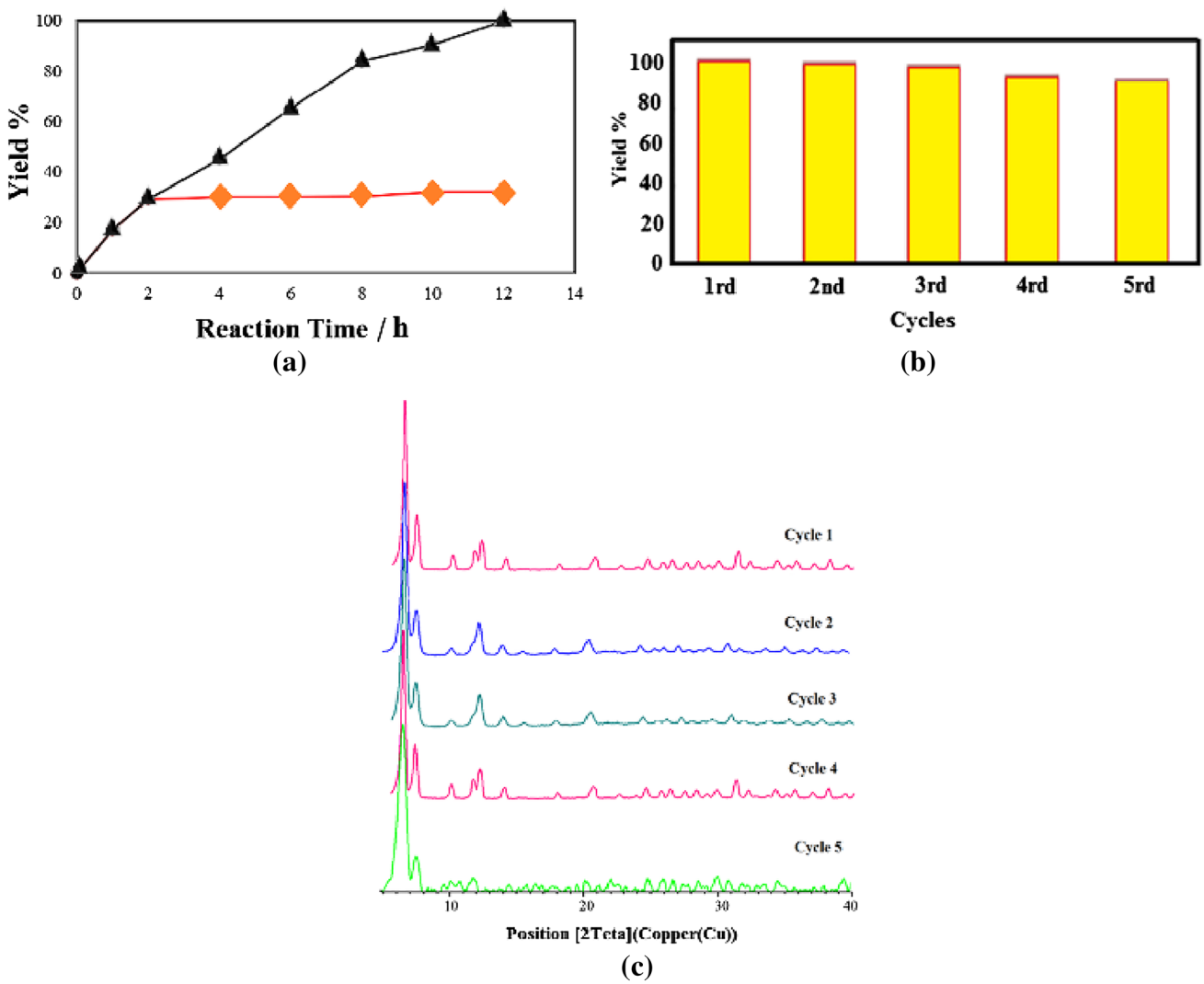

Fig. 4 **a** Leaching test of ZBU-Co, **b** recycle experiments of ZBU-Co for cycloaddition of CO_2 with ECH under solvent free, 6 h, 1 bar and room temperature condition. Conversion in each cycles: run 1, 100%; run 2, 99%; run 3, 98%; run 4, 97%; run 5, 95%; and **c** PXRD patterns of ZBU-Co after each catalytic cycles

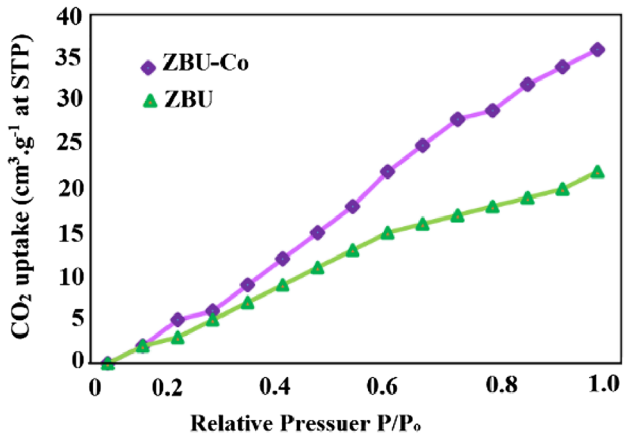

Fig. 5 CO_2 adsorption capability of ZBU and ZBU-Co at 298 K

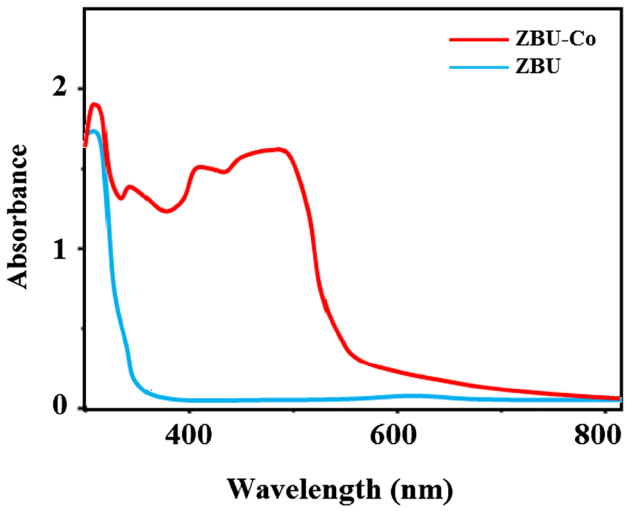

Fig. 6 UV–Vis diffuse reflectance spectra of Zr-Bipy-UiO-67-$Co(OAc)_2$ and Zr-Bipy-UiO-67

light to visible light. The Co-modified catalyst had higher light absorption intensity than the pristine MOF. Generally, enhanced light absorption is correlated with better catalytic activity [60].

Then, photocatalytic CO evolution experiments were performed under visible light illumination. When the photocatalytic CO_2 reduction was run with ZBU-Co and $Ru(Bipy)_3Cl_2$ (photosensitizer) for 4 h, 15.09 µmol CO was produced with a formation rate of 3452 µmol h^{-1} g^{-1} (Fig. 7a). In contrast, only a trace amount of CO was produced when ZBU was used, implying the versatility of the modified MOF. Further details regarding optimized conditions can be found in Table S1.

The chemical stability of the MOF was tested by a recyclability experiment (Fig. 7b). In good agreement with the PXRD patterns (Figure S1), the conversion ability of the ZBU-Co catalyst remained unchanged after four cycles. To gain insight into the electron transfer process of Co sites during CO_2 reduction, a photoluminescence (PL) experiment was carried out. Based on our findings, the emission intensity of the photosensitizer/ZBU-Co catalyst was significantly decreased compared to the photosensitizer/ZBU (Fig. 8). This can be ascribed to the fast electron transfer from the photosensitizer to the ZBU-Co, which further corroborates the combination of the photosensitizer/ZBU-Co in a photocatalytic system (Tables 2, 3).

Furthermore, the electron transfer in CO_2 reduction was further investigated by electrochemical testing (Fig. 9). As seen in Fig. 9, − 0.89 V (vs. Ag/AgCl) was recorded as the initial point for the increase in current density of ZBU-Co under CO_2 atmosphere compared to the current density of ZBU-Co under N_2 atmosphere. Therefore, − 0.89 V was recognized as the initial potential in the CO_2 reduction. Consequently, as − 1.31 V (vs. Ag/AgCl) has been recorded for singlet state of $E_s([Ru(bpy)_3]^{2+*}/[Ru(bpy)_3]^{3+}$ [61], it was

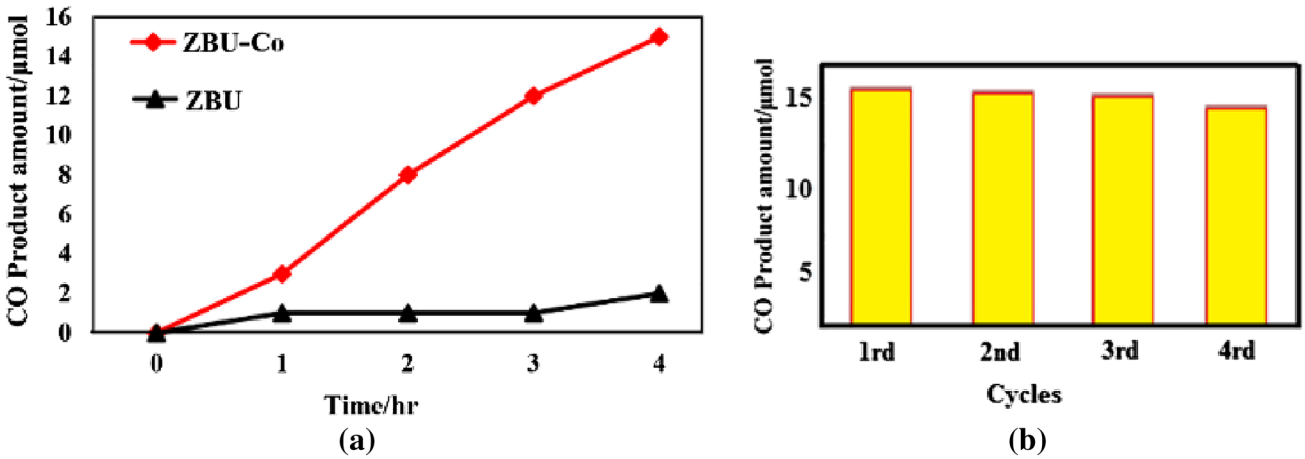

Fig. 7 **a** Monitoring CO evolution, **b** production yields of CO over ZBU-Co catalyst in four repeated cycles

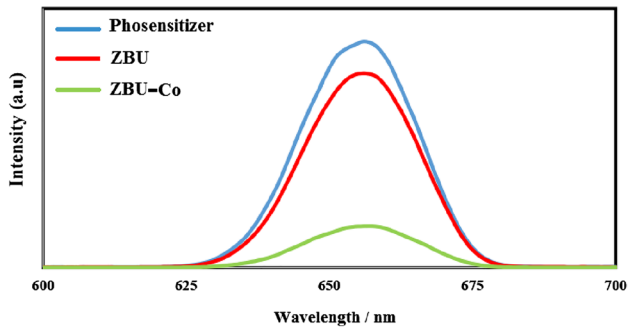

Fig. 8 PL spectra of photosensitizer before and after addition of ZBU and ZBU-Co

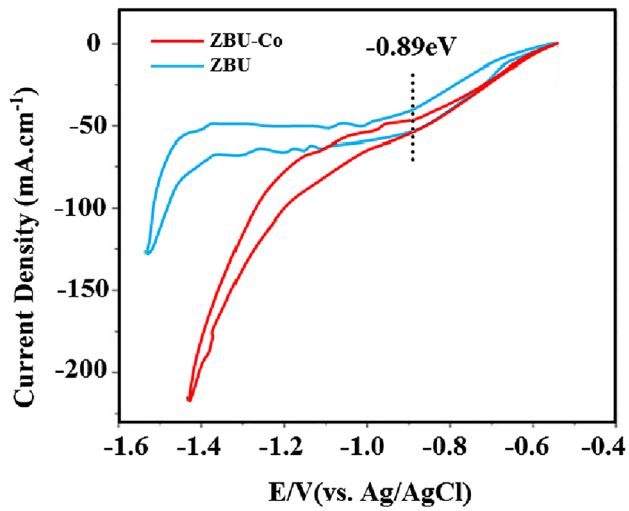

Fig. 9 CV of Zr-Bipy-UiO-67–Co(OAc)$_2$ under CO_2 and N_2

found that the CO_2 reduction is thermodynamically favorable ($\Delta G = -1.31$ V–(-0.89 V) $= -0.42$ V, i.e. <0) [62].

Moreover, the XPS analysis of ZBU-Co after photoreduction was not significantly altered, demonstrating the stability of the catalytic system (Figure S3). The mechanism of photocatalytic reduction is depicted in Fig. 10. In the first step, the photosensitizer is excited to produce $[Ru(bpy)_3]^{2+*}$. Then, electrons are transferred from the excited species $[Ru(bpy)_3]^{2+*}$ to ZBU-Co. As a result, ZBU-Co is reduced to $[ZBU\text{-}Co]^-$ and ($[Ru(bpy)_3]^{3+}$) is produced. Next, CO_2 molecules are reduced to CO by $[ZBU\text{-}Co]^-$. Finally, after the reaction of TEOA (triethanolamine) with ($[Ru(bpy)_3]^{3+}$ to form $TEOA^+/[Ru(bpy)3]^3+$, photocatalytic CO_2 reduction is completed and H_2 released as a side product [51] (Figure S3). Despite the feasibility of other side products such as formaldehyde, methanol, and hydrocarbons, the high selectivity of ZBU-Co towards CO production is remarkable. In MOFs, pores are the sites where catalysis and product formation take place. Therefore, product selectivity is controlled by pore size. In the case of ZBU-Co, it is believed that the pore

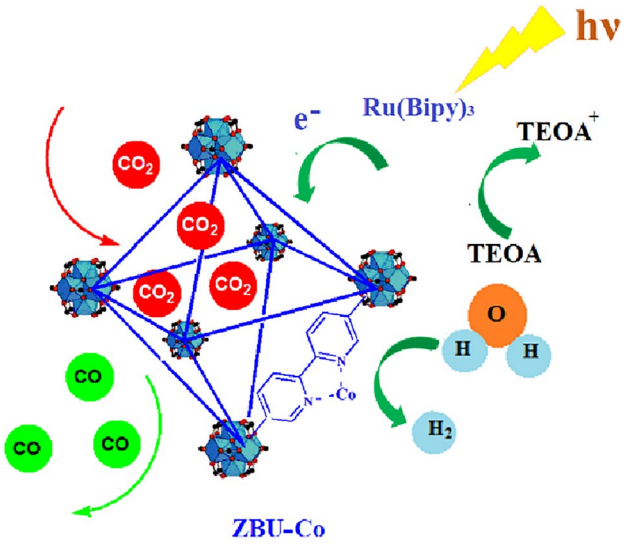

Fig. 10 The photocatalytic mechanism of the ZBU-Co for the conversion of CO_2 to CO

size of ZBU-Co is ideally suited for CO synthesis with high selectivity [44].

3 Conclusion

In summary, it is the first record of MOFs-catalyzed CO_2 transformation reactions with bifunctional catalysts. ZBU-Co can catalyze CO_2 insertion into epoxides under mild, green, solvent-free, and temperature-free conditions, achieving complete conversion. The CO_2 uptake capacity of the MOF was recorded at 36.7 $cm^3\ g^{-1}$, which is higher than the parent ZBU MOF (22.2 $cm^3\ g^{-1}$). Additionally, ZBU-Co was used for the photocatalytic reduction of CO_2 to CO under Xe lamp irradiation. The superior photocatalytic performance of ZBU-Co compared to the pristine ZBU is due to its higher charge transfer ability and CO_2 adsorption capacity. Moreover, the chemical stability and catalytic performance of the ZBU-Co remained unchanged after five cycles. Taken together, our findings open a new horizon for the rational design of efficient MOF catalysts, especially in the bi-functional mode for CO_2 transformation reactions.

Supplementary Information The online version contains supplementary material available at https://doi.org/10.1007/s10904-023-02860-0.

Author Contributions All authors contributed equally for producing the materials and contents for the manuscript.

Funding No funds, grants, or other support were received during the preparation of this manuscript.

Data Availability The datasets generated during the current study are available from the corresponding author on reasonable request.

Code Availability Not applicable.

Declarations

Conflict of interest The authors declare that they have no known competing financial interests or personal relationships that could have appeared to influence the work reported in the submitted manuscript.

References

1. V. Humphrey, J. Zscheischler, P. Ciais, L. Gudmundsson, S. Sitch, S.I. Seneviratne, Sensitivity of atmospheric CO2 growth rate to observed changes in terrestrial water storage. Nature **560**, 628–631 (2018)
2. B.J. Soden, W.D. Collins, D.R. Feldman, Reducing uncertainties in climate models. Science **361**, 326–327 (2018)
3. P. Yaashikaa, P.S. Kumar, S.J. Varjani, A. Saravanan, A review on photochemical, biochemical and electrochemical transformation of CO2 into value-added products. J. CO2 Util. **33**, 131–147 (2019)
4. N.L. Panwar, S.C. Kaushik, S. Kothari, Role of renewable energy sources in environmental protection: a review. Renew. Sust. Energ. Rev **15**, 1513–1524 (2011)
5. S. Chu, Y. Cui, N. Liu, The path towards sustainable energy. Nat. Mater. **16**, 16–22 (2017)
6. J. Raven, K. Caldeira, H. Elderfield, O. Hoegh-Guldberg, P. Liss, U. Riebesell, J. Shepherd, C. Turley, A. Watson, Ocean acidification due to increasing atmospheric carbon dioxide, R. Soc. (2005).
7. L. Kapsenberg, S. Alliouane, F. Gazeau, L. Mousseau, J.-P. Gattuso, Coastal ocean acidification and increasing total alkalinity in the northwestern Mediterranean Sea. Ocean Sci. **13**, 411–426 (2017)
8. E. Rabinowitch, Photosynthesis, US Atomic Energy Commission (1949).
9. J. Barber, Photosynthetic energy conversion: natural and artificial. Chem. Soc. Rev. **38**, 185–196 (2009)
10. C. Yoo, Y.-E. Kim, Y. Lee, Selective transformation of CO2 to CO at a single nickel center. Acc. Chem. Res. **51**, 1144–1152 (2018)
11. G. Mele, C. Annese, A. De Riccardis, C. Fusco, L. Palmisano, G. Vasapollo, L. D'Accolti, Turning lipophilic phthalocyanines/TiO2 composites into efficient photocatalysts for the conversion of CO2 into formic acid under UV–vis light irradiation. Appl. Catal. A Catal A **481**, 169–172 (2014)
12. C. Wu, F. Irshad, M. Luo, Y. Zhao, X. Ma, S. Wang, Ruthenium complexes immobilized on an azolium based metal organic framework for highly efficient conversion of CO2 into formic acid. ChemCatChem **11**, 1256–1263 (2019)
13. Y. Zhang, T. Zhang, S. Das, Catalytic transformation of CO 2 into C1 chemicals using hydrosilanes as a reducing agent. Green Chem. **22**, 1800–1820 (2020)
14. D. Hidalgo, J. Martín-Marroquín, Power-to-methane, coupling CO2 capture with fuel production: an overviewRenew. Sust. Energ. Rev **132**, 110057 (2020)
15. A. Yahaya, M. Gondal, A. Hameed, Selective laser enhanced photocatalytic conversion of CO2 into methanol. Chem. Phys. Lett. **400**, 206–212 (2004)
16. K. Yang, J. Jiang, Transforming CO2 into methanol with N-heterocyclic carbene-stabilized coinage metal hydrides immobilized in a metal–organic framework UiO-68. ACS Appl. Mater. Interfaces **13**, 58723–58736 (2021)
17. J.A. Rodriguez, P. Liu, D.J. Stacchiola, S.D. Senanayake, M.G. White, J.G. Chen, Hydrogenation of CO2 to methanol: importance of metal–oxide and metal–carbide interfaces in the activation of CO2. ACS Catal.Catal **5**, 6696–6706 (2015)
18. L. Wang, L. Wang, J. Zhang, X. Liu, H. Wang, W. Zhang, Q. Yang, J. Ma, X. Dong, S.J. Yoo, Selective hydrogenation of CO2 to ethanol over cobalt catalysts. Angew. Chem. Int. Ed. **57**, 6104–6108 (2018)
19. L. Liu, A.V. Puga, J. Cored, P. Concepción, V. Pérez-Dieste, H. García, A. Corma, Sunlight-assisted hydrogenation of CO2 into ethanol and C2+ hydrocarbons by sodium-promoted Co@C nanocomposites. Appl. Catal. B **235**, 186–196 (2018)
20. R. Motterlini, B.E. Mann, R. Foresti, Therapeutic applications of carbon monoxide-releasing molecules. Expert Opin. Invest. Drugs **14**, 1305–1318 (2005)
21. A. Nakao, Y. Toyoda, Application of carbon monoxide for transplantation. Curr Pharma Biotec **13**, 827–836 (2012)
22. E.V. Gusevskaya, J. Jiménez-Pinto, A. Börner, Hydroformylation in the realm of scents. ChemCatChem **6**, 382–411 (2014)
23. X. Yu, P.G. Pickup, Recent advances in direct formic acid fuel cells (DFAFC). J. Power. Sources **182**, 124–132 (2008)
24. J. Hietala, A. Vuori, P. Johnsson, I. Pollari, W. Reutemann, H. Kieczka, Formic acid. Ullmann's Encycl. Ind. Chem. **1**, 1–22 (2016)
25. G. Maggio, S. Freni, S. Cavallaro, Light alcohols/methane fuelled molten carbonate fuel cells: a comparative study. J. Power. Sources **74**, 17–23 (1998)
26. L. Spadaccini, M.C. Iii, Ignition delay characteristics of methane fuels. Prog. Energy Combust. Sci. Energy Combust. Sci **20**, 431–460 (1994)
27. S. Ma, P.J. Kenis, Electrochemical conversion of CO2 to useful chemicals: current status, remaining challenges, and future opportunities. Curr. Opin. Chem. Eng. **2**, 191–199 (2013)
28 M. Aresta, A. Dibenedetto, Utilisation of CO2 as a chemical feedstock: opportunities and challenges. Dalton Trans. **15**, 2975–2992 (2007)
29. E. Alper, O.Y. Orhan, CO2 utilization: developments in conversion processes. Petroleum **3**, 109–126 (2017)
30. S. Klaus, M.W. Lehenmeier, C.E. Anderson, B. Rieger, Recent advances in CO2/epoxide copolymerization: new strategies and cooperative mechanisms. Coord. Chem. Rev. **255**, 1460–1479 (2011)
31. N. Fanjul-Mosteirín, C. Jehanno, F. Ruipérez, H. Sardon, A.P. Dove, Rational study of DBU salts for the CO2 insertion into epoxides for the synthesis of cyclic carbonates. ACS Sustain. Chem. Eng. **7**, 10633–10640 (2019)
32. F. Norouzi, H.R. Khavasi, Diversity-oriented metal decoration on UiO-type metal–organic frameworks: an efficient approach to increase CO2 uptake and catalytic conversion to cyclic carbonates. ACS Omega **4**, 19037–19045 (2019)
33. L. Mohammadi, H.R. Khavasi, Anthracene-tagged UiO-67-MOF as highly selective aqueous sensor for nanoscale detection of arginine amino acid. Inorg. Chem. **59**, 13091–13097 (2020)
34. R. Babu, R. Roshan, A.C. Kathalikkattil, D.W. Kim, D.-W. Park, Rapid, microwave-assisted synthesis of cubic, three-dimensional, highly porous MOF-205 for room temperature CO2 fixation via cyclic carbonate synthesis. ACS Appl. Mater. Interfaces **8**, 33723–33731 (2016)
35. Z. Qin, H. Li, X. Yang, L. Chen, Y. Li, K. Shen, Heterogenizing homogeneous cocatalysts by well-designed hollow MOF-based nanoreactors for efficient and size-selective CO2 fixation. Appl. Catal. B Environ. **307**, 121163 (2022)
36. S.L. James, Metal-organic frameworks. Chem. Soc. Rev. **32**, 276–288 (2003)
37. P. Horcajada, C. Serre, M. Vallet-Regí, M. Sebban, F. Taulelle, G. Férey, Metal–organic frameworks as efficient materials for drug delivery. Angew. Chem. Chem **118**, 6120–6124 (2006)

38. J. Lee, O.K. Farha, J. Roberts, K.A. Scheidt, S.T. Nguyen, J.T. Hupp, Metal–organic framework materials as catalysts. Chem. Soc. Rev. **38**, 1450–1459 (2009)
39. K. Lu, T. Aung, N. Guo, R. Weichselbaum, W. Lin, Nanoscale metal–organic frameworks for therapeutic, imaging, and sensing applications. Adv. Mater. **30**, 1707634 (2018)
40. F. Norouzi, H.R. Khavasi, Iodine decorated-UiO-67 MOF as a fluorescent sensor for the detection of halogenated aromatic hydrocarbons. New J. Chem. **44**, 8937–8943 (2020)
41. Q. Qian, P.A. Asinger, M.J. Lee, G. Han, K.M. Rodriguez, S. Lin, F.M. Benedetti, A.X. Wu, W.S. Chi, Z.P. Smith, MOF-based membranes for gas separations. Chem. Rev. **120**, 8161–8266 (2020)
42. C. Petit, Present and future of MOF research in the field of adsorption and molecular separation. Curr. Opin. Chem. Eng. **20**, 132–142 (2018)
43. J.H. Cavka, S. Jakobsen, U. Olsbye, N. Guillou, C. Lamberti, S. Bordiga, K.P. Lillerud, A new zirconium inorganic building brick forming metal organic frameworks with exceptional stability. J. Am. Chem. Soc. **130**, 13850–13851 (2008)
44. A.H. Vahabi, F. Norouzi, E. Sheibani, M. Rahimi-Nasrabadi, Functionalized Zr-UiO-67 metal-organic frameworks: Structural landscape and application. Coord. Chem. Rev. **445**, 214050 (2021)
45. A. Helal, F. Alahmari, M. Usman, Z.H. Yamani, Chalcopyrite UiO-67 metal-organic framework composite for CO2 fixation as cyclic carbonates. J. Environ. Chem. Eng. **10**, 108061 (2022)
46. L.-G. Ding, B.-J. Yao, W.-L. Jiang, J.-T. Li, Q.-J. Fu, Y.-A. Li, Z.-H. Liu, J.-P. Ma, Y.-B. Dong, Bifunctional imidazolium-based ionic liquid decorated UiO-67 type MOF for selective CO2 adsorption and catalytic property for CO2 cycloaddition with epoxides. Inorg. Chem. **56**, 2337–2344 (2017)
47. E.S. Gutterød, S. Øien-Ødegaard, K. Bossers, A.-E. Nieuwelink, M. Manzoli, L. Braglia, A. Lazzarini, E. Borfecchia, S. Ahmadigoltapeh, B. Bouchevreau, B.T. Lønstad-Bleken, R. Henry, C. Lamberti, S. Bordiga, B.M. Weckhuysen, K.P. Lillerud, U. Olsbye, CO2 Hydrogenation over Pt-containing UiO-67 Zr-MOFs: the base case. Ind. Eng. Chem. Res. **56**, 13206–13218 (2017)
48. D. Jiang, Y. Shi, G. Zhao, X. Gong, J. Liu, D. Lan, L. Zhang, J. Ge, H. Fang, D. Cheng, Pt–Ni alloy nanobead chains catalysts embedded in UiO-67 membrane for enhanced CO2 conversion to CO. Mater. Today Energy **28**, 101051 (2022)
49. X. Zhao, M. Xu, X. Song, X. Liu, W. Zhou, H. Wang, P. Huo, Tailored linker defects in UiO-67 with high ligand-to-metal charge transfer toward efficient photoreduction of CO2. Inorg. Chem. **61**, 1765–1777 (2022)
50. H. Xu, X. Luo, J. Wang, Y. Su, X. Zhao, Y. Li, Spherical sandwich Au@ Pd@ UIO-67/Pt@ UIO-n (n= 66, 67, 69) core–shell catalysts: Zr-based metal–organic frameworks for effectively regulating the reverse water–gas shift reaction. ACS Appl. Mater. Interfaces **11**, 20291–20297 (2019)
51. X. Gao, B. Guo, C. Guo, Q. Meng, J. Liang, J. Liu, Zirconium-based metal–organic framework for efficient photocatalytic reduction of CO2 to CO: the influence of doped metal ions. ACS Appl. Mater. Interfaces **12**, 24059–24065 (2020)
52. S. Subudhi, D. Rath, K. Parida, S. Satyabrata, D. Rath, K.M. Parida, A mechanistic approach towards the photocatalytic organic transformations over functionalised metal organic frameworks: a review. Catal. Sci. Technol.. Sci. Technol **8**, 679–696 (2018)
53. P. Behera, S. Subudhi, S.P. Tripathy, K. Parida, MOF derived nano-materials: A recent progress in strategic fabrication, characterization and mechanistic insight towards divergent photocatalytic applications. Coord. Chem. Rev.. Chem. Rev **456**, 214392 (2022)
54. J. Panda, S.P. Tripathy, S. Dash, A. Ray, P. Behera, S. Subudhi, K. Parida, Inner transition metal-modulated metal organic frameworks (IT-MOFs) and their derived nanomaterials: a strategic approach towards stupendous photocatalysis. Nanoscale **15**, 7640–7675 (2023)
55. S.P. Tripathy, S. Subudhi, K. Parida, Inter-MOF hybrid (IMOFH): a concise analysis on emerging core–shell based hierarchical and multifunctional nanoporous materials. Coord. Chem. Rev. **434**, 213786 (2021)
56. J. Qin, S. Wang, X. Wang, Visible-light reduction CO2 with dodecahedral zeolitic imidazolate framework ZIF-67 as an efficient co-catalyst. Appl. Catal. B **209**, 476–482 (2017)
57. W. Liu, L. Zhang, W. Yan, X. Liu, X. Yang, S. Miao, W. Wang, A. Wang, T. Zhang, Single-atom dispersed Co–N–C catalyst: structure identification and performance for hydrogenative coupling of nitroarenes. Chem. Sci. **7**, 5758–5764 (2016)
58 Y. Shi, S. Hou, X. Qiu, B. Zhao, MOFs-based catalysts supported chemical conversion of CO2. Metal-Organic Framew. **8**, 373–426 (2020)
59. Q.-L. Zhu, J. Li, Q. Xu, Immobilizing metal nanoparticles to metal–organic frameworks with size and location control for optimizing catalytic performance. J. Am. Chem. Soc. **135**, 10210–10213 (2013)
60. H. Li, Y. Gao, Z. Xiong, C. Liao, K. Shih, Enhanced selective photocatalytic reduction of CO2 to CH4 over plasmonic Au modified g-C3N4 photocatalyst under UV–vis light irradiation. Appl. Surf. Sci. **439**, 552–559 (2018)
61. Y. Gao, L. Ye, H. Chen, L. Sun, Highly efficient photocatalytic reduction of CO2 and H2O to CO and H2 with a cobalt bipyridyl complex. J. Energy Chem. **27**, 502–506 (2018)
62. T. Ouyang, H.H. Huang, J.W. Wang, D.C. Zhong, T.B. Lu, A dinuclear cobalt cryptate as a homogeneous photocatalyst for highly selective and efficient visible-light driven CO2 reduction to CO in CH3CN/H2O solution. Angew. Chem. **129**, 756–761 (2017)